INTERNATIONAL JOURNAL FOR NUMERICAL METHODS IN FLUIDS
Int. J. Numer. Meth. Fluids 2001; **37**: 933–949 (DOI: 10.1002/fld.198)

The composite finite volume method on unstructured meshes for the two-dimensional shallow water equations

Wang Jiwen[a,b,*,1] and Liu Ruxun[a,2]

[a] *Department of Mathematics, University of Science and Technology of China, Hefei, China*
[b] *Department of Computer Science and Engineering, Anhui University, Hefei, China*

SUMMARY

A composite finite volume method (FVM) is developed on unstructured triangular meshes and tested for the two-dimensional free-surface flow equations. The methodology is based on the theory of the remainder effect of finite difference schemes and the property that the numerical dissipation and dispersion of the schemes are compensated by each other in a composite scheme. The composite FVM is formed by global composition of several Lax–Wendroff-type steps followed by a diffusive Lax–Friedrich-type step, which filters out the oscillations around shocks typical for the Lax–Wendroff scheme. To test the efficiency and reliability of the present method, five typical problems of discontinuous solutions of two-dimensional shallow water are solved. The numerical results show that the proposed method, which needs no use of a limiter function, is easy to implement, is accurate, robust and is highly stable. Copyright © 2001 John Wiley & Sons, Ltd.

KEY WORDS: composite scheme; finite volume method; Lax–Friedrichs scheme; Lax–Wendroff scheme; numerical remainder effect; shallow water wave problems; unstructured triangular meshes

1. INTRODUCTION

The study on the shallow water wave problems by the numerical method is one of the most active topics in computational mathematics, computational fluid mechanics and computational hydraulics. Using numerical simulation and numerical analysis, taking the suitable simplified model, scientists can get a lot of significant information for various complicated shallow water wave phenomena. In recent years, especially, many impressive and wonderful numerical simulated results for two-dimensional or three-dimensional discontinuous problems are continually reported.

* Correspondence to: Department of Mathematics, University of Science and Technology of China, Hefei, Anuhui 230026, China.
[1] E-mail: wangw@mail.ustc.edu.cn
[2] E-mail: liurx@ustc.edu.cn

Received 9 February 2000
Revised 11 October 2000

Various numerical methods have been developed for the numerical simulation of shallow water wave problems, such as the finite difference method, characteristic method, finite element method, grid type method, spectral method and finite volume method (FVM) and so on. In recent years, FVM has attracted wide attention and has a series of successes in the numerical simulation of two-dimensional shallow water wave problems. Using Roe's Riemann solver, Alcrudo and Carcia-Navarro [1] developed a high-resolution Godunov-type MUSCL-FVM and reported impressive results for rapidly varying inviscid flow. Zhao *et al.* [2] using Osher's scheme [3], designed a FVM on unstructured meshes. Anastasiou and Chan [4,5] introduced a Roe-type second-order-accurate upwind FVM on unstructured triangular meshes. Using a Harten–Lax–van Leer (HLL) Riemann solver, Hu *et al.* [6] developed an HLL-type MUSCL-FVM. Tseng [7] proposed an explicit FVM, which takes the Roe, TVD and ENO method as the special case respectively.

Recently, Liska and Wendroff [8] reported the composite scheme for two-dimensional shallow water equations, which combined Lax–Wendroff (LW) and Lax–Friedrich (LF) into a multi-steps composite scheme. It is well known that both LW and LF have mutual opposite drawbacks in their dissipation and dispersion effects. The LW scheme is a second-order accurate scheme, but its high numerical dispersive effect will produce oscillation close to shocks. The LF scheme is non-oscillatory but has an overextending numerical dissipation effect [9–11]. A composite scheme combines these two methods into a step-by-step scheme to exploit their merits and remove their deficiencies. One example of a composite scheme is a global composition of several LW steps followed by one diffusive LF step, which serves as a consistent filter removing the unwanted oscillations. This simple construction is efficient and produces surprisingly good results. By comparison, the method in [8] is a finite difference scheme (FDS) on a regular trapezoidal mesh only, this bringing a serious restriction to the application of the method.

In this paper, a composite FVM on unstructured triangular meshes is advanced. Since the method is designed on unstructured meshes, it is able to handle problems with arbitrary complexity domains. Five typical problems of discontinuous solutions of two-dimensional shallow water, including the classical dam break problems and supercritical channel flow problems, are solved by the present method. The numerical results show that the proposed method, which needs no use of a limiter function and is easily to implement, is accurate, robust and highly stable.

The paper is organized as follows. Section 2 presents the shallow water equations in two dimensions. Section 3 describes the composite finite volume discretization of two-dimensional shallow water equations on the unstructured triangular meshes, the criterion for numerical stability and the boundary conditions used. In Section 4, the numerical results of several two-dimensional steady and unsteady flows with discontinuities are given to validate and demonstrate the usefulness and the good features of the schemes. Finally, a discussion and concluding remarks are given in the last two sections.

2. TWO-DIMENSIONAL SHALLOW WATER EQUATIONS

Under the assumption of an incompressible, constant pressure distribution on free surface, with neglecting wind, Coriolis forces and horizontal internal shear stresses, the

two-dimensional shallow water equation can be expressed in conservation laws as follows:

$$U_t + (F(U))_x + (G(U))_y = S$$

where U is the vector of conservative variables, $F(U)$ and $G(U)$ are the flow fluxes

$$U = \begin{bmatrix} h \\ hu \\ hv \end{bmatrix}, \qquad F = \begin{bmatrix} hu \\ hu^2 + \frac{1}{2}gh^2 \\ huv \end{bmatrix}, \qquad G = \begin{bmatrix} hv \\ huv \\ hv^2 + \frac{1}{2}gh^2 \end{bmatrix}$$

h is the depth of water, u and v are the depth-averaged velocity components in the x-direction and y-direction respectively, g the gravitational acceleration, S a source term, due to the friction losses and bed slopes. In the present study, only the homogeneous case is considered ($S = 0$). The Jacobian matrices of the fluxes F and G are

$$A = \begin{bmatrix} 0 & 1 & 0 \\ gh - u^2 & 2u & 0 \\ -uv & v & u \end{bmatrix}, \qquad B = \begin{bmatrix} 0 & 0 & 1 \\ -uv & v & u \\ gh - v^2 & 0 & 2v \end{bmatrix}$$

with eigenvalues $\{u, u \pm \sqrt{gh}\}$ and $\{v, v \pm \sqrt{gh}\}$ respectively.

3. NUMERICAL METHODS

3.1. One-dimensional composite finite difference schemes

For a system of conservation laws

$$U_t = f_x(U)$$

the two-step LF scheme on a staggered grid is defined as

$$U_{i+1/2}^{n+1/2} = \frac{1}{2}[U_i^n + U_{i+1}^n] + \frac{\Delta t}{2\Delta x}[f(U_{i+1}^n) - f(U_i^n)] \tag{1}$$

$$U_i^{n+1} = \frac{1}{2}[U_{i-1/2}^{n+1/2} + U_{i+1/2}^{n+1/2}] + \frac{\Delta t}{2\Delta x}[(U_{i+1/2}^{n+1/2}) - f(U_{i-1/2}^{n+1/2})] \tag{2}$$

The LW scheme employs Richtmyer's two-step algorithm. The first step uses the same predictor (1), the second step takes the leap-frog scheme

$$U_i^{n+1} = U_i^n + \frac{\Delta t}{\Delta x}\left[f(U_{i+1/2}^{n+1/2}) - f(U_{i-1/2}^{n+1/2})\right] \tag{3}$$

It is well know that the LW scheme produces oscillations in the vicinity of shocks, while LF is excessively diffusive, smearing out the shocks.

The composite scheme is defined by global composition through with $k-1$ LW steps followed by one LF step. The operator defined by the LW scheme (1) and (3) is denoted L_{W}, and the operator defined by the LF scheme (1) and (2) by L_{F}, with both operators doing one time step from time level n to $n+1$. Then, the difference operator S_k is defined as

$$S_k = L_{\mathrm{F}} \circ L_{\mathrm{W}} \circ \cdots \circ L_{\mathrm{W}} \tag{4}$$

and the composite scheme is called LWLFk

$$U^{n+k} = S_k U^n \tag{5}$$

The numerical solutions obtained by LWLFk not only maintain the sharpness of shocks, but also have no oscillations.

3.2. Composite finite volume method on unstructured triangular meshes

Consider the system of conservation laws in two dimensions

$$U_t = f_x(U) + g_y(U)$$

The composite finite volume methods on unstructured triangular meshes are constructed as follows. By the Green's formula, we have

$$f_x + g_y = \frac{1}{A}\iint f_x + g_y \,\mathrm{d}x\,\mathrm{d}y = \frac{1}{A}\oint f\,\mathrm{d}y - g\,\mathrm{d}x \tag{6}$$

The standard way of FVM takes (6) as the basic device of approximating $f_x + g_y$ in a suitable control volume, where A is the area of the domain of integration. The two-step predictor–corrector method is also adopted. The conservative variables are stored at the nodes of the meshes, while the predictor conservative variables are stored at the centres of the triangular elements of the meshes. The algorithm corresponding to one-dimensional LF scheme is still called LF, but the one corresponding to LW is called a new name CF, which means the corrector LF scheme. Similar to one-dimensional, the composite schemes formed by $k-1$ steps of CF followed by one step of LF are denoted CFLFk.

3.2.1. LF predictor. Suppose the solution region is triangulated into an unstructured mesh, let $c(i)$ is the ith triangular cell, the three vertices of $c(i)$ are counterclockwise denoted by $g(i, 0)$, $g(i, 1)$, $g(i, 2)$, the corresponding co-ordinates are (x_0, y_0), (x_1, y_1), (x_2, y_2) respectively. The area of $c(i)$ is denoted $S_{c(i)}$. The circumcentre (simply called centre hereafter) of $c(i)$ is also denoted $c(i)$. The area of the sub-triangle $\Delta_{c(i)g(i,1)g(i,2)}$, which is opposite to the grid $g(i, 0)$, is denoted $s(i, 0)$. Similar meanings are referred by $s(i, 1)$, $s(i, 2)$ respectively (see Figure 1).

Then the LF predictor is calculated as follows:

$$\begin{aligned} S_{c(i)}U^{n+1/2}_{c(i)} &= s(i,0)U^n_{g(i,0)} + s(i,1)U^n_{g(i,1)} + s(i,2)U^n_{g(i,2)} \\ &\quad + \frac{\Delta t}{2}[F_{01}(y_1 - y_0) + F_{12}(y_2 - y_1) + F_{20}(y_0 - y_2) - G_{01}(x_1 - x_0) - G_{12}(x_2 - x_1) \\ &\quad - G_{20}(x_0 - x_2)] \end{aligned} \tag{7}$$

where the fluxes F and G are given by

$$F_{kl} = f(U^{n+1/4}_{kl}), \qquad G_{kl} = g(U^{n+1/4}_{kl})$$

and $U^{n+1/4}$ takes a suitable approximate solution of an appropriate one-dimensional Riemann problem, for example, the LF approximation of the Riemann problem at each edge of $c(i)$

$$\begin{aligned} U^{n+1/4}_{01} &= \frac{1}{2}(U^n_{g(i,0)} + U^n_{g(i,1)}) \\ &\quad + \frac{\Delta t}{4}\frac{(f(U^n_{g(i,1)}) - f(U^n_{g(i,0)}))(x_1 - x_0) + (g(U^n_{g(i,1)}) - g(U^n_{g(i,0)}))(y_1 - y_0)}{(x_1 - x_0)^2 + (y_1 - y_0)^2} \end{aligned} \tag{8}$$

3.2.2. LF corrector. Let $g(i)$ is the ith grid point of the mesh, the co-ordinate of $g(i)$ is (x_g, y_g). In an unstructured mesh, the number of the neighbouring cells of a node, generally speaking, is not fixed. Without loss of generality, the number of the neighbouring cells of the node $g(i)$ is assumed to be six. The neighbouring cells of $g(i)$ are counterclockwise denoted by

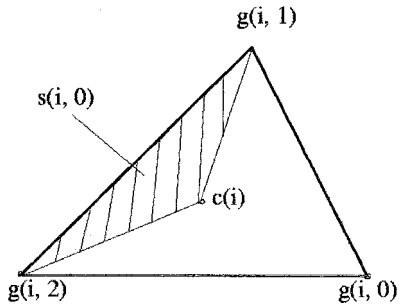

Figure 1. A cell and the notation used in the LF predictor.

$c(i, 0), c(i, 1), \ldots, c(i, 5)$, and the corresponding centre co-ordinates are denoted by $(x_0, y_0), (x_1, y_1), \ldots, (x_5, y_5)$ respectively. The area of the convex polygon $c(i, 0), c(i, 1), \ldots, c(i, 5)$ is denoted $S_{g(i)}$. The control volume and the notation used in the LF corrector are shown in Figure 2.

Then the LF corrector is

$$U_{g(i)}^{n+1} = \frac{1}{\sum_{j=0}^{5} d_j} \sum_{j=0}^{5} d_j U_{c(i,j)}^{n+1/2} + \frac{\Delta t}{2S_{g(i)}} [F_{01}(y_1 - y_0) + F_{12}(y_2 - y_1) + \cdots + F_{50}(y_0 - y_5) - G_{01}(x_1 - x_0) - G_{12}(x_2 - x_1) - \cdots - G_{50}(x_0 - x_5)] \tag{9}$$

where d_j and the fluxes F and G are given by

$$d_j = (\sqrt{(x_j - x_g)^2 + (y_j - y_g)^2})^{-1} \quad (j = 0, 1, \ldots, 5), \quad F_{kl} = f(U_{kl}^{n+3/4}), \quad G_{kl} = g(U_{kl}^{n+3/4})$$

and

$$U_{01}^{n+3/4} = \frac{1}{2}(U_{c(i,0)}^{n+1/2} + U_{c(i,1)}^{n+1/2}) + \frac{\Delta t}{4} \frac{(f(U_{c(i,1)}^{n+1/2}) - f(U_{c(i,0)}^{n+1/2}))(x_1 - x_0) + (g(U_{c(i,1)}^{n+1/2}) - g(U_{c(i,0)}^{n+1/2}))(y_1 - y_0)}{(x_1 - x_0)^2 + (y_1 - y_0)^2} \tag{10}$$

3.2.3. CF corrector. The CF predictor is the same as the LF predictor (7). The control volume and the notation used in the construction of the CF corrector scheme are the same ones used in the LF corrector (shown in Figure 2). By (6) and using the trapezoidal integral approximation of f and g along the edges, the CF corrector is

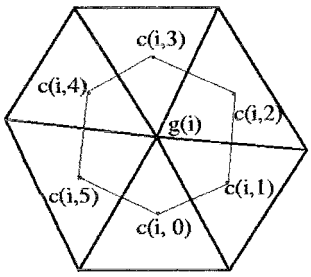

Figure 2. The control volume and the notation used in the LF corrector.

$$
\begin{aligned}
U_{g(i)}^{n+1} = U_{g(i)}^{n} + \frac{\Delta t}{2S_{g(i)}} & [(f(U_{c(i,0)}^{n+1/2}) + f(U_{c(i,1)}^{n+1/2}))(y_1 - y_0) + \cdots \\
& + (f(U_{c(i,5)}^{n+1/2}) + f(U_{c(i,0)}^{n+1/2}))(y_0 - y_5) - (g(U_{c(i,0)}^{n+1/2}) + g(U_{c(i,1)}^{n+1/2}))(x_1 - x_0) - \cdots \\
& - (g(U_{c(i,5)}^{n+1/2}) + g(U_{c(i,0)}^{n+1/2}))(x_0 - x_5)] \\
= U_{g(i)}^{n} + \frac{\Delta t}{2S_{g(i)}} & \left[\sum_{j=0}^{5} f(U_{c(i,j)}^{n+1/2})(y_{j+1} - y_{j-1}) - \sum_{j=0}^{5} g(U_{c(i,j)}^{n+1/2})(x_{j+1} - x_{j-1}) \right] \qquad (11)
\end{aligned}
$$

where set $x_{-1} = x_5$, $x_6 = x_0$, $y_{-1} = y_5$, $y_6 = y_0$.

3.3. Numerical stability

The scheme proposed here is an explicit scheme, which is restricted by a CFL-like condition on the time step. In view of the eigenvalues of the Jacobian matrices of the two fluxes in two-dimensional shallow water equations are $\{u, u \pm \sqrt{gh}\}$ and $\{v, v \pm \sqrt{gh}\}$ respectively, the criterion adopted in this paper is

$$
\Delta t \leq \frac{\min\{d_i\}}{\max\{(|u \pm \sqrt{gh}|)_i, (|v \pm \sqrt{gh}|)_i\}}
$$

In the above inequality, the quantities d_i represent the whole set of distances between arbitrary two neighbouring centrepoints.

3.4. Boundary conditions

At the inflow boundary, some constant values of h, u, v on the boundary are given. At the free boundaries, the transmissive boundary conditions are used. The transmissive boundaries are obtained by setting $h_n = 0$, $u_n = 0$, $v_n = 0$, where the subscript n denotes the derivative along the normal vector $\vec{n}$ of the boundary. At the solid wall boundaries, we use free-slip and no-permeable boundary conditions, setting $h_n = 0$, $(u, v)\cdot\vec{n} = 0$.

4. NUMERICAL RESULTS

In this section, the numerical results are shown. There are several test problems that validate and illustrate how the composite FVMs work for the two-dimensional shallow water problems.

4.1. Two-dimensional dam break problem

Two two-dimensional dam break tests are examined. The dam problems are rapidly varying unsteady flows and provide extreme cases to examine the numerical stability and the efficiency of the scheme.

4.1.1. Two-dimensional partial dam break problem. This test has been computed in several recent papers [1,2,4,12]. The geometry of the problem consists of a 200×200-m^2 basin as illustrated in Figure 3. The initial water level of the upstream of the dam is 10 m and the tail

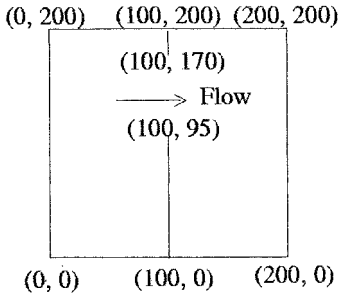

Figure 3. Definition of problem domain for partial dam break test.

water is 5 m high. At the instant of dam failure, water is released into the downstream side through a breach 75 m wide, creating a bore wave that moves while spreading laterally. At the same time a depression wave, or rarefaction wave, propagates upstream. The problem domain was triangulated into 5722 cells (see Figure 4).

Calculation is done by the CFLF4. The computational model was run up to 7.2 s after the dam break. Figures 5 and 6 show the three-dimensional view of the water surface elevation and the contour map of water depths respectively. These results agree well with those reported in [1,2,4,12].

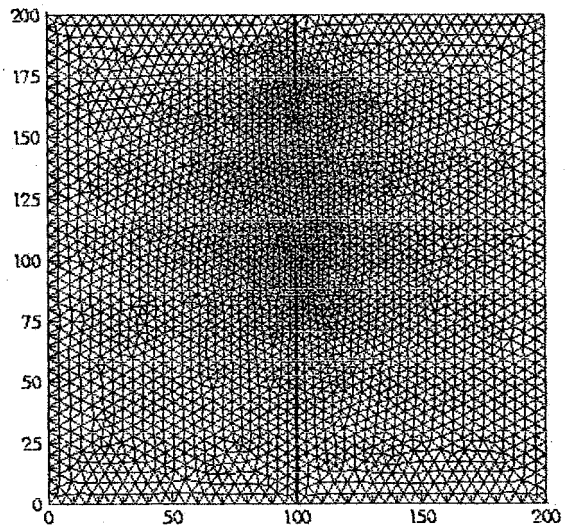

Figure 4. The unstructured mesh for partial dam break test.

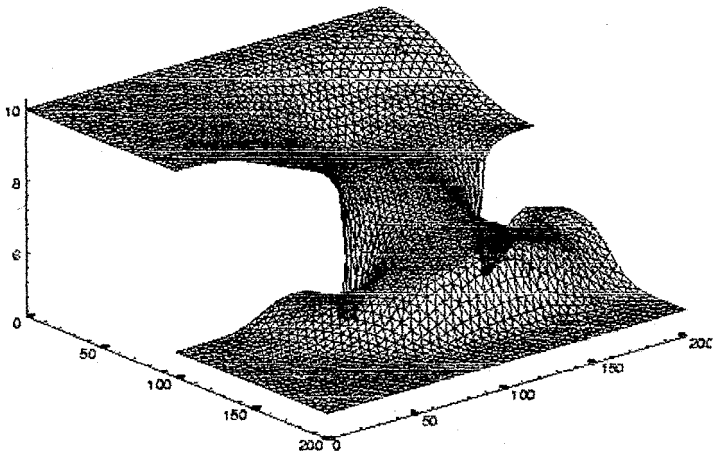

Figure 5. Water surface profile at $t = 7.2$ s after breaking of dam.

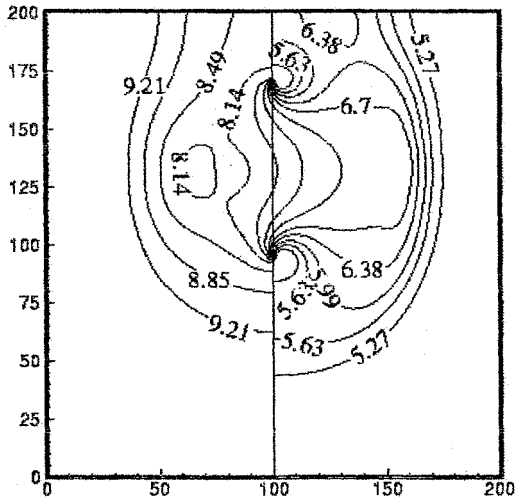

Figure 6. Contour plot of water elevation for partial dam break test.

4.1.2. Circular dam break problem. This problem was first solved in [1] then also in [4,7,8]. The problem domain is a square (0, 50 m) × (0, 50 m). In the centre of the square is a cylindrical dam with radius 11 m. The initial water level is 10 m inside the dam and 1 m outside the dam and water is initially at rest.

Suddenly, the dam disappears and then the waves radially spread. The computational domain was triangulated into 5790 cells (see Figure 7), and the model was run for up to 0.69 s after the dam break. Calculation is done by the CFLF7. Figures 8 and 9 show the numerical results for the water surface elevation in three- and two-dimensions respectively. The plots show that the circular symmetry is well preserved. In general, the contours of water surface elevation appear in good agreement with those reported in [1,4,7,8].

4.2. Supercritical channel flows

These supercritical (Froude number $F_r = \sqrt{u^2 + v^2}/\sqrt{gh} > 1$) flow test cases include flows through the channel with wall constrictions. Their solution is a steady state flow with hydraulic and negative jumps.

4.2.1. Oblique hydraulic jump. The oblique hydraulic jump is induced by means of an interaction between a supercritical flow and a converging wall deflected through an angle $\alpha = 8.95°$. The stock wave is formed with an angle β. This problem is a very useful standard test for two-dimensional hydraulic flow modelling because the exact solution is available. The definition of the problem domain and a schematic diagram of the induced shock front are show in Figure 10.

The initial and inflow conditions are the height $h_0 = 1$ m, velocity $u_0 = 8.57$ m s^{-1} and $v_0 = 0$. Fixed boundary conditions are applied at the upstream boundary. Transmissive boundary conditions are imposed at the downstream boundary and slip and no-pass boundary conditions at the channel walls. The computational domain was triangulated into 2683 cells (see Figure 11), and the model was run to steady state. Calculation is done by the CFLF7. The

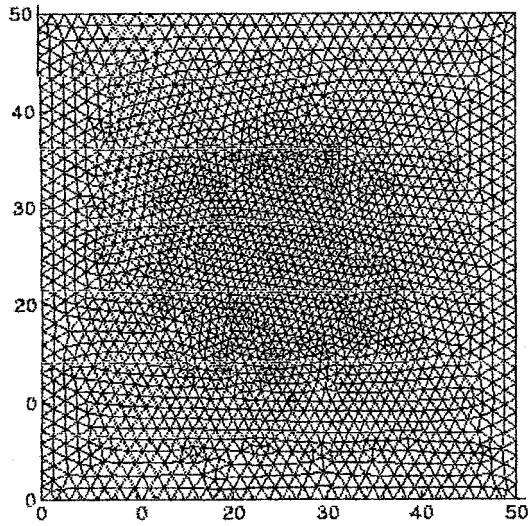

Figure 7. The unstructured mesh for circular dam break test.

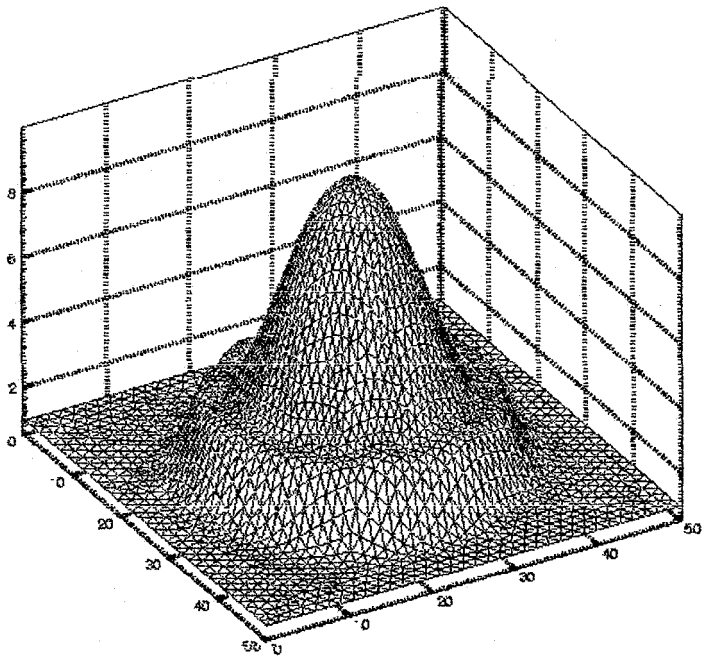

Figure 8. Water surface profile at $t = 0.69$ s after breaking of circular dam.

depth contour plot of the steady state solution is shown in Figure 12. The angle, formed by the shock front with the x-axis, $\beta \approx 30°$ from the numerical solution agrees well with the analytic results $\beta = 30°$ [1]. Also, the numerical height and velocity $h_2 = 1.501$ m, $|u_2| = 7.9567$ m s^{-1}, agree well with the analytical prediction $h_2 = 1.5$ m, $|u_2| = 7.9556$ m s^{-1} [1].

4.2.2. Symmetric channel constriction. In this test case, the channel wall is symmetrically constricted from both side with angle $\alpha = 5°$. The initial and inflow conditions are the height $h_0 = 1$ and Froude number $F_r = 2.5$. The computational domain was triangulated into 4627 cells (see Figure 13), and the model was run to steady state. Calculation is done by the CFLF9. Figures 14 and 15 show the numerical results for the water surface elevation in three- and two-dimensions respectively.

In this case, again, they can compare numerical results with analytic ones. Numerical values of the heights $h_2 = 1.256$, $h_3 = 1.558$ of the first and second plateau agree well with analytical results $h_2 = 1.25$, $h_3 = 1.55$ [8].

4.2.3. Symmetric channel with variable width. In this test case, the channel wall is symmetrically constricted from both sides with angle $\alpha = 15°$ and past the constriction there follows again a

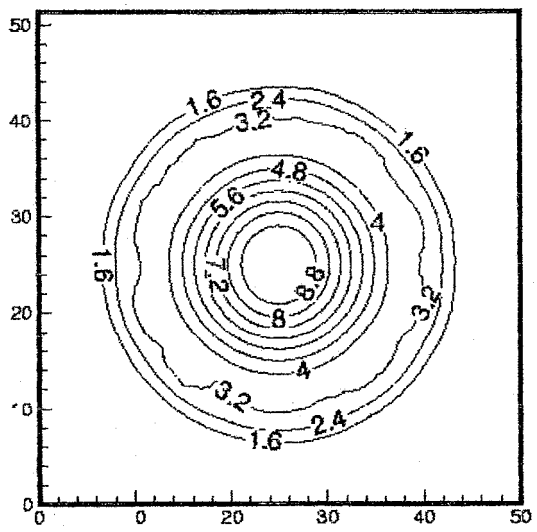

Figure 9. Contour plot of water elevation for circular dam break test.

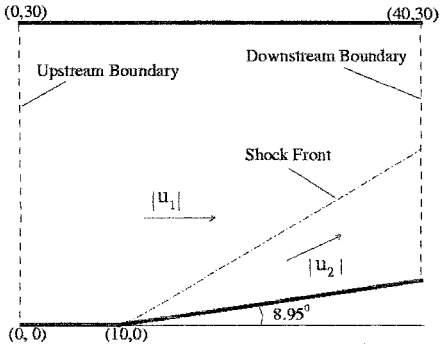

Figure 10. Sketch of oblique hydraulic jump.

straight narrower channel. The geometry of the problem with an unstructured mesh of 4493 cells is given in Figure 16.

The initial and inflow conditions are the height $h_0 = 1$ and Froude number $F_r = 2.5$. Calculation is done by the CFLF8, and the model was run to steady state. Figures 17 and 18 show the numerical results for the water surface elevation in three- and two-dimensions respectively.

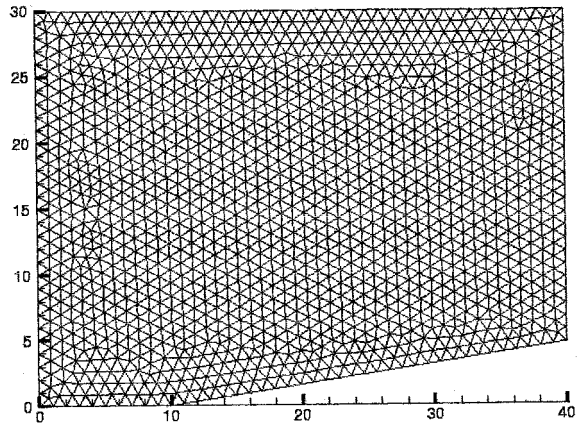

Figure 11. The unstructured mesh for oblique hydraulic jump test.

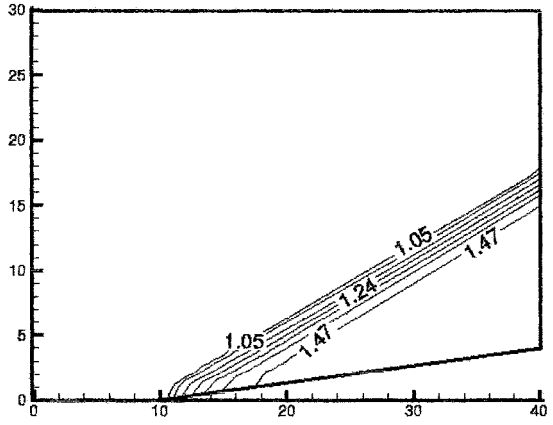

Figure 12. Water surface profile showing oblique hydraulic jump.

The results are similar to those in [8], and show again a cross-wave pattern that includes not only hydraulic jumps as in the previous examples, but also negative jumps that are caused by the presence of concave corners.

5. DISCUSSION

Early in 1968, Fromm *et al.* [13,14] discovered the composite effect of FDS by means of adjusting numerical dissipation effect and numerical dispersion effect and proposed an

approach to eliminate or constrain the numerical dispersion efficiency of FDS by a similar composite idea. Their famous works attracted a lot of attention. In 1974, Warming *et al.* [15] systematically developed the theory of remainder analysis of FDS and provided a theoretical basis for the reforming, improving and optimizing of FDS. The design and successful applications of the MacCormack scheme and the λ-scheme, the good performance of the composite scheme in [8] and in this paper all show that the composite approach by using mutual-opposite-effect schemes is directional and successful.

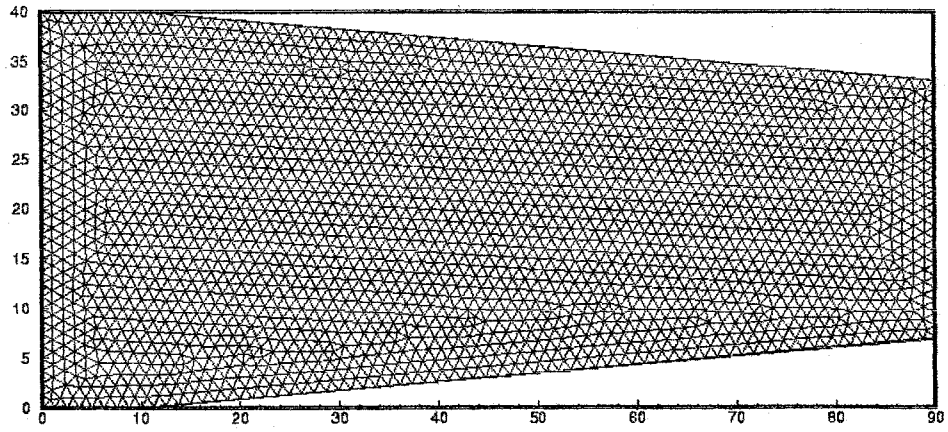

Figure 13. Geometry and the unstructured mesh for the symmetry channel constriction problem.

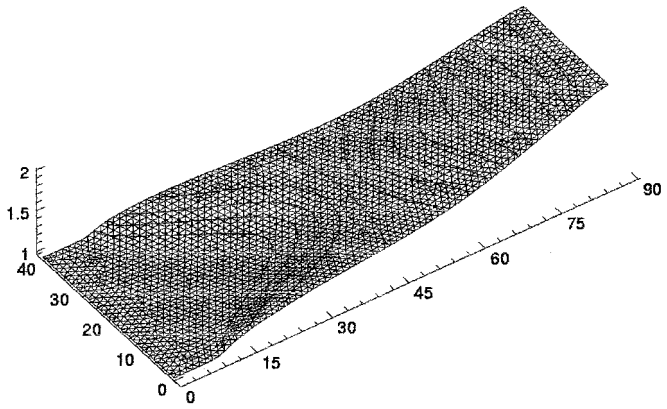

Figure 14. Water surface profile for the symmetry channel constriction problem.

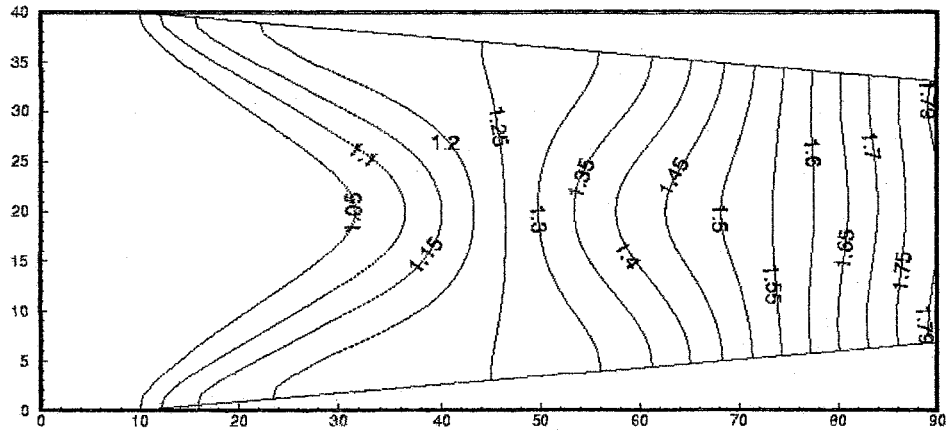

Figure 15. Contour plot of water elevation for the symmetry channel constriction problem.

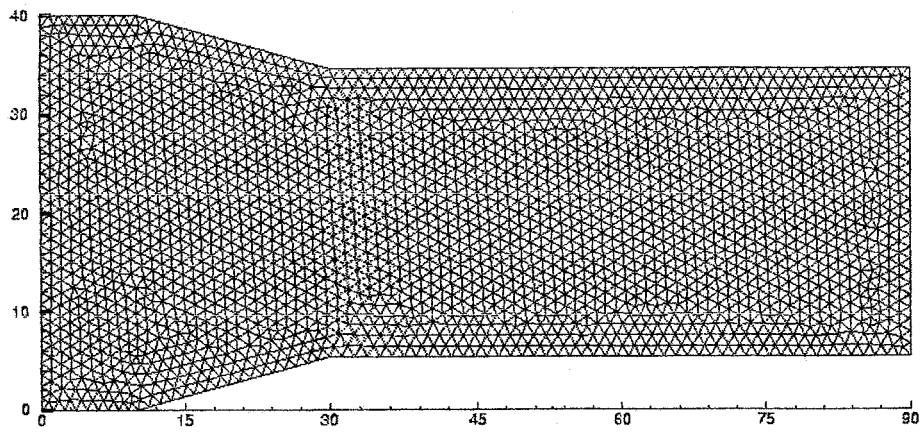

Figure 16. Geometry and the unstructured mesh for the symmetry channel with variable width problem.

6. CONCLUSIONS

A versatile, easily to implement, composite finite volume method for the two-dimensional shallow water equations has been developed for unstructured triangular meshes and tested. The method is formed by global composition of several Lax–Wendroff type multi-step followed by a Lax–Friedrich step, need no use of a limiter, and is able to attain an adequate accuracy by adjusting the number of times of applying the two schemes which have counter remainder effects. The scheme has been applied to the two-dimensional dam breaking

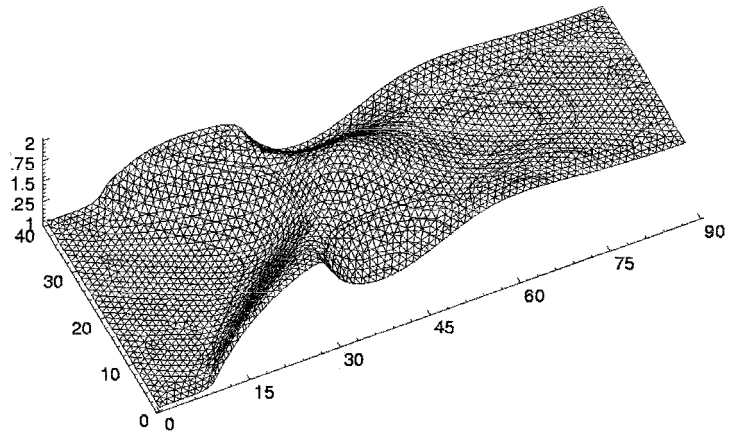

Figure 17. Water surface profile for the symmetry channel with variable width problem.

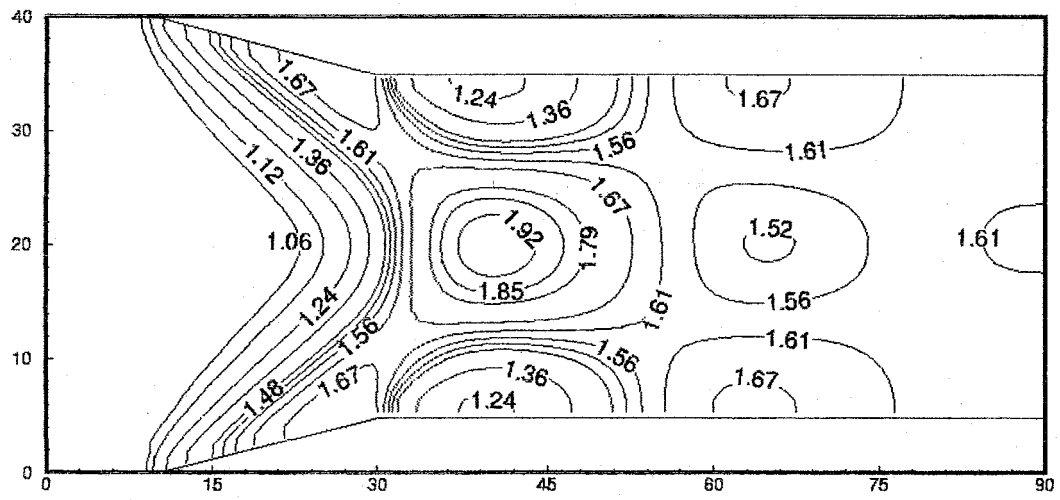

Figure 18. Contour plot of water elevation for the symmetry channel with variable width problem.

problems and the supercritical channel flows. The numerical results show that the method is stable, highly flexible, able to handle a wide range of flow regimes and able to capture shock well. From the authors' experience, the scheme is a rather fast algorithm. So, the method is preferred for practical applications when computation time, overall accuracy and applicability are considered.

ACKNOWLEDGMENTS

This work was supported by NSF of America grant INT-96011084 and NNSF of China grant 10071083.

REFERENCES

1. Alcrudo F, Garcia-Navarro P. A high-resolution Godunov-type scheme in finite volumes for the 2D shallow-water equations. *International Journal for Numerical Methods in Fluids* 1993; **16**: 489–505.
2. Zhao DH, Shen HW, TabiousIII GQ, Lai JS, Tan WY. Finite-volume two-dimensional unsteady flow model for river basins. *ASCE Journal of Hydraulic Engineering* 1994; **120**: 864–883.
3. Osher S, Solomone F. Upwind difference schemes for hyperbolic systems of conservation laws. *Mathematics in Computing* 1982; **38**: 339–374.
4. Anastasiou K, Chan CT. Solution of the 2D shallow water equations using the finite volume method on unstructured triangular meshes. *International Journal for Numerical Methods in Fluids* 1997; **24**: 1225–1245.
5. Chan CT, Anastasiou K. Solution of incompressible flows with or without a free surface using the finite volume method on unstructured triangular meshes. *International Journal for Numerical Methods in Fluids* 1999; **29**: 35–57.
6. Hu K, Mingham CG, Causon DM. A bore-capturing finite volume method for open-channel flows. *International Journal for Numerical Methods in Fluids* 1998; **28**: 1241–1261.
7. Tseng MS. Explicit finite volume non-oscillatory schemes for 2D transient free-surface flows. *International Journal for Numerical Methods in Fluids* 1999; **30**: 831–843.
8. Liska R, Wendroff B. Two-dimensional shallow water equations by composite schemes. *International Journal for Numerical Methods in Fluids* 1999; **30**: 467–479.
9. Liu RX, Zhang MP, Wang J, Liu XY. The designing approach of difference schemes by controlling the remainder-effect. *International Journal for Numerical Methods in Fluids* 1999; **31**: 523–533.
10. Liu RX. On the nonlinear computation stability. *Acta Mechanica Sinica* 1984; **5**: 529 (in Chinese).
11. Liu RX, Zhou ZH. The remainder-effect analysis of FDS and the applications. *Applied Mathematics and Mechanics* 1995; **16**: 87–96.
12. Fennema RJ, Chaudhry MH. Explicit methods for 2D transient free-surface flows. *Journal of Hydraulic Engineering ASCE* 1990; **116**: 1013–1034.
13. Fromm JE. A method for reducing dispersion in convective difference schemes. *Journal of Computational Physics* 1968; **3**: 176–189.
14. Hirt CW. Heuristic stability theory for finite difference equations. *Journal of Computational Physics* 1968; **2**: 339–355.
15. Warming RF, Hyett BJ. The modified equation approach to the stability and accuracy analysis of finite difference methods. *Journal of Computational Physics* 1974; **14**: 159–179.

